Spectrochimica Acta Part A: Molecular and Biomolecular Spectroscopy 157 (2016) 227–237

Contents lists available at ScienceDirect

Spectrochimica Acta Part A: Molecular and Biomolecular Spectroscopy

journal homepage: www.elsevier.com/locate/saa

Conformational study and reassessment of the vibrational assignments for Norspermidine

T.M. Silva [a], S.M. Fiuza [a], M.P.M. Marques [a,b], L.A.E. Batista de Carvalho [a], A.M. Amado [a,*]

[a] I&D Unit "Química-Física Molecular", Department of Chemistry, Faculty of Science and Technology, University of Coimbra, P-3004-535 Coimbra, Portugal
[b] Department of Life Sciences, University of Coimbra, 3000-456 Coimbra, Portugal

ARTICLE INFO

Article history:
Received 12 October 2015
Accepted 4 January 2016
Available online 8 January 2016

Keywords:
Norspermidine
Vibrational spectroscopy
Conformational preferences
Quantum chemical calculations
Dielectric constant effect

ABSTRACT

The present study presents and discusses the conformational preferences of Norspermidine (NSpd). The effects of varying the dielectric constant on the conformational preferences are discussed, with a view to infer which conformation will correspond to the most stable in the pure condensed liquid phase. Within the same context, a set of NSpd-NH_3 molecular adducts were simulated in order to determine the relevance of intermolecular hydrogen bonding on the overall stability and relative positioning of the respective vibrational frequencies.
The calculations presently performed allowed a reassessment of the vibrational assignments for NSpd. A full assignment of the NSpd vibrational spectra is presented, with special emphasis being given to the vibrational modes that proved to be most affected by hydrogen bonding. The various inconsistencies of a prior study found in the literature were identified and rectified.

1. Introduction

Polyamines, such as putrescine [$H_2N(CH_2)_4NH_2$, Put], spermidine [$H_2N(CH_2)_3NH(CH_2)_4NH_2$, Spd] and spermine [$H_2N(CH_2)_3NH(CH_2)_4NH(CH_2)_3NH_2$, Spm], are found in most living cells in millimolar concentrations. At physiological pH conditions these systems are N-protonated, thus behaving as intrinsic polycations. A bewildering maze of cellular functions has been ascribed to these important biogenic compounds. They were shown to be essential in eukaryotic cell growth and differentiation, as well as in the maintenance of the native structure of different biological macromolecules [1–5]. Since deregulated polyamine metabolism is recognized as a characteristic of animal cancers [4,6–8], interference with the polyamine biosynthetic pathways seems to be a very promising therapeutical approach against proliferative diseases [9–11].

The accidental discovery of the antitumor properties of cisplatin (*cis*-diamminedichloroplatinum(II), hereafter named as cDDP; Scheme 1) by Rosenberg et al. [12–14], prompted a growing interest towards the development of new metal-based anticancer drugs. The finding led to a renewed interest in the field of polyamines, which have become potential substituent groups for the replacement of the cDDP NH_3 ligands in cDDP aiming at the design of new cisplatin-like anticancer drug candidates [15,16].

In recent years, the authors have been interested in the understanding of the structure–activity relationships (SARs) that underline the antineoplastic activity of some platinum(II) and palladium(II) complexes with linear alkylpolyamines. The structural characterization of both polyamine ligands and metal complexes has been mainly performed by vibrational spectroscopy (Raman, inelastic neutron scattering (INS) and infrared) coupled to quantum chemical calculations [17–30]. One of the polyamines that has been considered is norspermidine (bis(3-aminopropyl)amine, $H_2N(CH_2)_3NH(CH_2)_3NH_2$, NSpd; Scheme 2), a modified polyamine structurally related to the biogenic polyamine spermidine (N-(3-aminopropyl)-1,4-butanediamine), Spd; Scheme 2). The cytotoxic potential of NSpd and of its Pt(II)- and Pd(II)-complexes has been evaluated [31], with quite promising results.

Regarding the vibrational characterization of NSpd, to the best of our knowledge only one attempt has been reported [23]. However, the vibrational assignments performed in that work are based on computational results obtained from calculations that, besides considering the incorrect form of NSpd form (the fully protonated one, which is definitely not the species occurring in pure condensed liquid phase), evidence significant inconsistencies. Hence, the herein reported work presents a comprehensive conformational study on NSpd, based on calculations that consider the non-protonated NSpd form and use the correct combination between molecular charge and multiplicity. The report culminates in a thorough reassessment of the vibrational assignment of the experimental FT-Raman and FTIR spectra.

2. Experimental and computational details

NSpd was purchased from Sigma-Aldrich Chemical Co (Sintra, Portugal) and used without further purification.

* Corresponding author.
E-mail address: amado.am@gmail.com (A.M. Amado).

http://dx.doi.org/10.1016/j.saa.2016.01.003
1386-1425/

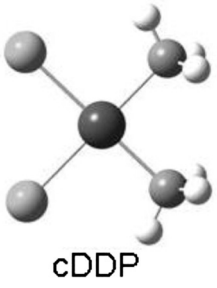

Scheme 1. Molecular structure of cisplatin.

2.1. FTIR spectroscopy

The Attenuated Total Reflection Infrared (ATR-FTIR) spectra were recorded on an IFS 55 spectrometer, using a Golden Gate single reflection diamond ATR system, with no need for sample preparation. All spectra are the average of two counts of 128 scans each. A spectral resolution of 2 cm^{-1} was used in all cases.

2.2. FT-Raman spectroscopy

The FT-Raman spectra were recorded on a RFS-100 Bruker FT-spectrometer, using a Nd:YAG laser with excitation wavelength of 1064 nm. The laser power was set to 150 mW. Each spectrum is the averaging of two repeated measurements of 100 scans each at 2 cm^{-1} resolution.

2.3. Quantum chemical calculations

Optimization and vibrational gas-phase calculations were performed using the Gaussian 09w program (G09w) [32], installed in a PC machine. The hybrid DFT functional denoted by mPW1PW was used combined with the widely used 6-31G* electron basis set. The authors are aware of the smallness of the all electron basis set used. Its use is, nevertheless, justified for two main reasons. First, this work is enclosed within a wide project that aims to study polyamines, of progressively greater size and complexity, and the corresponding metal complexes. Given that comparisons are intended, it is desirable to maintain uniform the theoretical level considered. Moreover, an increase of the theoretical level complexity can quickly make quantum chemical calculations prohibitive, as the number of electrons of the system increases. On the other hand, the mPW1PW/6-31G* theory level has proven to yield reliable results for different amines and corresponding metal complexes, at the expense of an acceptable level of computational demands [18,20,22,26,28,29,33].

All geometries were submitted to full geometry optimization without any symmetry constraints, and subsequently to a vibrational frequency calculation to confirm its correspondence to a real minimum in the NSpd potential energy surface (no negative eigenvalue) and to quantify the zero-point vibrational energy correction (zpve).

In order to infer on the effects of the dielectric constant on the conformational preferences of NSpd, SCRF calculations (optimization and frequency) were performed within the PCM formalism (polarized continuum model). All default parameters were used except the radii model which was set as UAHF (for more details see [26]). This combination between Gaussian program version, SCRF formalism and atomic radii model has proven to yield good results for isopropylamine (iPram) [26]. In the current study a wide variety of common solvents were selected in order to contemplate a broad range of dielectric constant values (at 25 °C). The full list of solvents considered and the corresponding dielectric constants [32,34] are given in Table S1 (Supplementary Material).

NBO analyses [35–37], as implemented in G09W [32], were also carried out for the optimized geometries, at selected dielectric constant values, in order to get a deeper insight into their electronic structures. Special attention was given to NBO Wiberg bond orders, dipole moments and second-order stabilization energies.

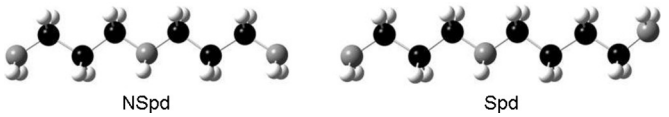

Scheme 2. Molecular structures of Norspermidine and Spermidine.

3. Results and discussion

3.1. Conformational analysis

Similarly to other linear alkylpolyamines, NSpd presents a high skeletal flexibility due to free rotation around the six skeletal dihedral angles, thus allowing a huge variety of possible molecular geometries. The most common values observed for the skeletal dihedral angles are 60° (*gauche*, **G**), 180° (*trans*, **T**) and −60° (*gauche′*, **G′**). An identical variability (60° (**g**), 180° (**t**) and −60° (**g′**)) is found for the three LpN–CC torsional angles, Lp standing for nitrogen lone pair.

Theoretically, regarding only the skeletal torsional angles variability, there are 729 possibilities for the NSpd core structure. Due to centrosymmetry of NSpd and conformational degenerescence, the number of distinct possibilities is significantly reduced. From the 361 distinct molecular geometries assembled and submitted to optimization, a total of 270 were found to correspond to stable conformers (no negative eigenvalue) within the potential energy surface of NSpd. The remaining molecular structures either converged to one of the former or proved to be a saddle point (one negative eigenvalue). It should be noted that the variability of the LpN–CC torsional angles was not explicitly evaluated since it is hypothesised that, as no constraint is imposed, they will adopt the conformation leading to the greatest stability in the view of the overall skeleton configuration.

The gas-phase (isolated molecule) conformational study predicts the 270 conformers of NSpd to be distributed within a relative stability range of *ca.* 39 kJ mol^{-1}, after zpve correction. Fig. 1 presents the variation of the relative stability (ΔE_{rel}) of the 13 most stable conformers which are found to lie within a range of 10 kJ mol^{-1}. The relative position of the almost-fully *trans* conformation (tTTTg′TTTt), which occupies the 22nd position of the ranking ($\Delta E_{rel} \approx 12$ kJ mol^{-1}) is included for the reason referred above. The molecular structures of the 14 conformers are presented in Fig. S1 (Supplementary Material) together with the conformational profile of both skeletal and LpN–CC torsional angles, and the H···N distances of the potentially stabilizing intramolecular N–H···N hydrogen bonds. The LpN–CC torsional angle concerning the central amine group (NH) is not indicated from now on, as the definition of the two skeletal torsional angles on both sides restrict the possibilities to g or g′.

The higher stability seems to be guaranteed by the occurrence of a t-g′-g′ profile of the three LpN–CC torsional angles and a GG′T (or G′GT) skeletal configuration for at least one side of NSpd, taking the NH-group at the molecular middle (Fig. 1). The most stable conformer presents the GG′T skeletal conformation on both molecular sides (tGG′T-TG′Gg′). The higher stability is ensured by two intramolecular N–H···N contacts, namely N_t–H···N (222.7 pm) and N_c–H···N′ (214.8 pm), where N_t and N_c stand for the terminal and central nitrogen atoms, respectively (Fig. S1). The coexistence of the two hydrogen bonds assures a higher stability for the tGG′T-TG′Gg′ conformation of over 4.5 kJ mol^{-1}, relatively to the second most stable conformer, tTG′T-TG′Gg′ (Fig. 1).

One property known to affect the relative stability of conformers is the medium dielectric constant. NSpd solutions with a variety of solvents (Table S1 of the Supplementary Material) were simulated, by

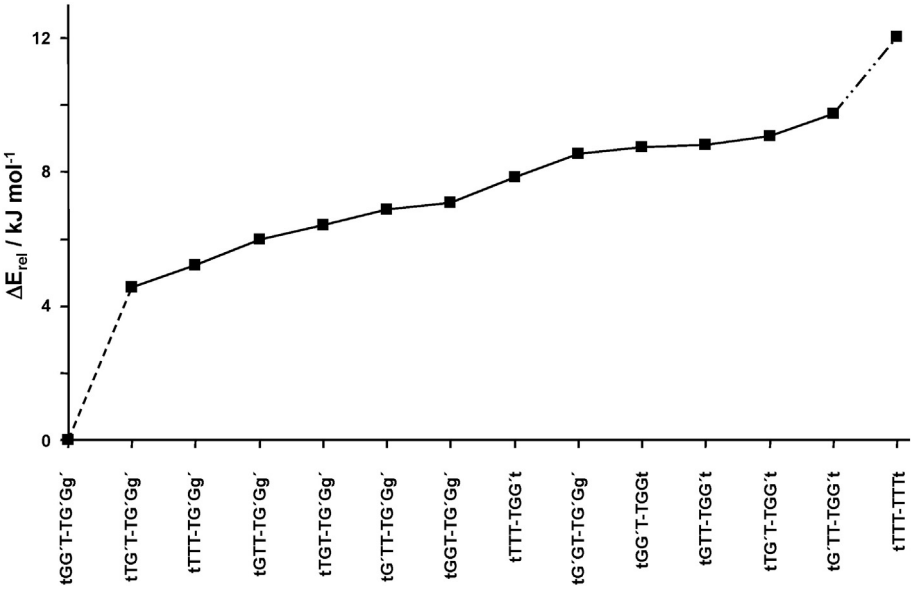

Fig. 1. Variation of the gas-phase relative stability (ΔE_{rel}) of the 13 most stable conformers (ΔE_{rel} within the range of 10 kJ mol^{-1}). The tTTT-TTTt conformer, expected to be the most stable in the condensed phase, is also included for comparison.

considering medium dielectric constant (ε) values ranging from 1 (vacuum; calculations for the isolated molecule) to 186 (N-methyl-formamide as solvent). The variation of the relative stabilities of two selected NSpd conformations (tTTT-TTTt and tGG′T-TG′Gg) was thus analysed as a function of the ε values. The tTTT-TTTt conformation was considered alongside with the tGG′T-TG′Gg, as it corresponds to the most stable conformation in the condensed liquid phase [17,19,38–41].

Fig. 2 presents the variation profile of the relative stability of the tTTT-TTTt conformer with respect to the tGG′T-TG′Gg′ one (ΔE_{rel}, in kJ mol^{-1}), as a function of the ε value. By definition, positive ΔE_{rel} values indicate a higher stability of the tGG′T-TG′Gg′ conformer whereas a negative value corresponds to a tTTT-TTTt greater stability. Curve fitting attempts showed that the best global adjustment is achieved with a second order exponential decay curve described as:

$$\Delta E_{rel} = -11.190 + 8.097 \times e^{-(\varepsilon/14.553)} + 25.967 \times e^{-(\varepsilon/1.910)}$$

The associated R^2 is 0.9995, meaning that about 99.95% of the observed ΔE_{rel} decay (*i.e.*, tTTT-TTTt stability increment relatively to tGG′T-TG′Gg′) is explained by variation in medium dielectric constant. According to the fitting equation, an inversion of the relative stability between the two conformers is expected to occur at a ε-value of ≈3.258. This value will be referred to as the threshold value from now on.

In an attempt to understand the loss of stability of the tGG′T-TG′Gg′ conformer in relation to the tTTT-TTTt one, the length variations of the two stabilizing intramolecular interactions (N_t–H···N_c and N_c–H···N_t′) were assessed as a function of the dielectric constant. The distances in the isolated state (vacuum phase) were used as reference, being the length variations ($\Delta_{H\cdots N}$; pm) determined as $\Delta_{H\cdots N} = d_{H\cdots N}(\text{vacuum}) - d_{H\cdots N}(\varepsilon)$. Therefore, a negative value of $\Delta_{H\cdots N}$ means an increase of the H···N distance on passing from the vacuum to a medium with a dielectric constant value ε > 1.

Fig. 3 presents the plots of $\Delta_{H\cdots N}$ values of both N–H···N interactions, as a function of ε value. The effect of the dielectric constant is found to be significantly more pronounced for the N_c–H···N_t′ interaction than for the N_t–H···N_c (Fig. 3). As for the ΔE_{rel}, in both cases the best fitting was achieved considering second-order exponential decay relationships. The fitting equations determined for the N_t–H···N and

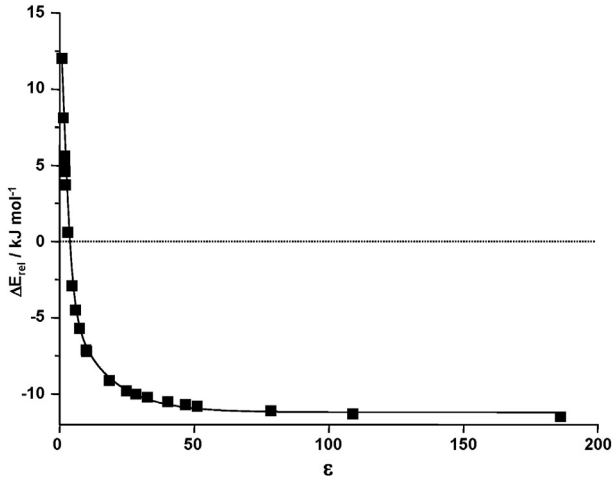

Fig. 2. Variation of relative stability (ΔE_{rel}) of the tTTT-TTTt conformer with respect to the conformer found to be the most stable in the gas-phase (tGG′T-TG′Gg′) as a function of dielectric constant (ε).

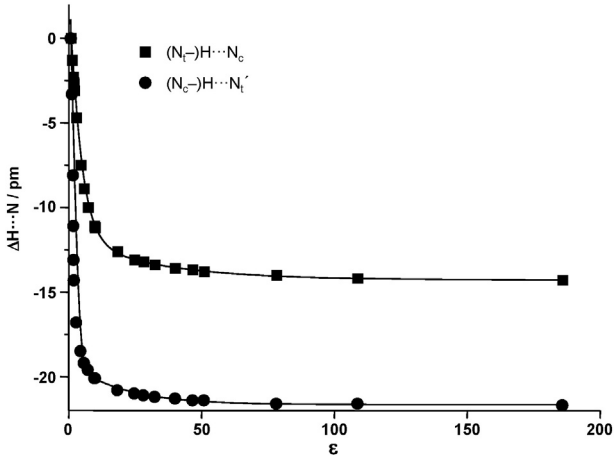

Fig. 3. Variation of the H···N distance (ΔH···N, pm) of the N_t–H···N_c and N_c–H···N_t′ hydrogen bonds in conformer tGG′T-TG′Gg′ as a function of dielectric constant (ε). The H···N distance predicted in the vacuum (ε = 1) is considered as reference.

N_c–H⋯N′ interactions are

$$\Delta_{H\cdots N} = -14.290 + 2.531 \times e^{-(\varepsilon/32.3616)} + 15.332 \times e^{-(\varepsilon/3.978)} \quad R^2 = 0.9998$$

and

$$\Delta_{H\cdots N} = -21.657 + 2.553 \times e^{-(\varepsilon/19.863)} + 50.011 \times e^{-(\varepsilon/1.113)} \quad R^2 = 0.9807,$$

respectively. Considering the threshold ε-value, the $\Delta_{H\cdots N}$ values for the N_t–H⋯N_c and N_c–H⋯N_t′ interactions are predicted to assume values of *ca.* −5.24 and −16.81 pm, respectively. In other words, at a ε-value of 3.258 the N_t–H⋯N_c and N_c–H⋯N_t′ hydrogen bond distances are expected to be lengthened from about 223 and 215 pm (in the vacuum, Fig. S1) to *ca.* 228 and 232 pm, respectively. SCRF calculation performed for the tGG′T-TG′Gg′ conformation at ε = 3.258 retrieved (N_t–)H⋯N_c and (N_c–)H⋯N_t′ distances of 227.7 and 231.9 pm, respectively, clearly validating the fitting equations found.

Attempting to rationalize the effects underlying the lengthening predicted for the stabilizing hydrogen bonds with dielectric constant increase, NBO calculations were performed considering different values of ε. Special attention was given to the most significant second-order stabilization energies, dipole moments and Wiberg bond orders. Table 1 compiles the selected results as a function of conformer (tGG′T-TG′Gg′ and tTTT-TTTt) and dielectric constant (Table S1).

Starting with the second-order stabilization energies, the most relevant difference between the two conformers is the absence of the stabilizing delocalization between nitrogen electron lone pair and N–H antibonding sigma orbital $LpN_c \rightarrow \sigma^*N_t$–H and $LpN_t \rightarrow \sigma^*N_c$–H in the tTTT-TTTt, regardless of the ε-value. In the vacuum, these orbital interactions contribute with a stabilization of 24 and 33 kJ mol^{-1}, respectively, in the tGG'T-TG'Gg′ conformation. Increasing dielectric constant promotes a gradual decrease of this stabilizing effect. At threshold ε-value the contribution of those orbital delocalizations are predicted to be reduced by over 12 and 39%, respectively. The relevance of these orbital interactions for conformer stability has already been stressed out for other kind of aliphatic amines [25,42].

A similar behaviour is observed for the variation of the Wiberg bond indexes related to the (N_t–)H⋯N_c and (N_c–)H⋯N_t′ interactions. Increase of dielectric constant from 1.00 (vacuum) to 3.258 reduces the H⋯N_c and H⋯N_t′ Wiberg indexes by *ca.* 3% and *ca.* 25%, respectively. The sharper decrease predicted for both 2nd–order stabilization energy and Wiberg index of the N_c–H⋯N_t′ interaction in comparison to the N_t–H⋯N_c interaction is in line with the relative effects observed for the $\Delta_{H\cdots N}$. (Fig. 3).

Regarding the dipole moments, increasing dielectric constant leads to an increase of the net dipole moment and delocalization contributions, regardless of the conformer. In both cases, the largest delocalization contribution to the dipole moment relates to the electron lone pairs of the nitrogen atoms. There is, however, a clear difference between the two conformers with respect to the variation profile of the delocalization contribution to the total dipole moment. In the case of the tTTT-TTTt conformer, the delocalization contribution gradually increases with dielectric constant, leading to an enhancement of the total dipole moment. In the case of the tGG′T-TG′Gg′ the opposite is predicted.

The delocalization contributions tend to decrease as the medium dielectric constant increases. This leads to a smoothing of dipole moment increase with ε, as evidenced by the increasing proximity between net and total values of dipole moment. This distinct behaviour can at least

Table 1
Comparison of selected NBO results for the *tTTTg′TTTt* and *tGG′Tg′TG′Gg′* conformers.

NBO Parameter[a]	ε									
	1.00	2.228	3.0473	3.258[b]	4.7113	10.125	32.613	46.826	78.3553	186.0
Second-order stabilization energies[c]					*tTTTg′TTTt*					
$LpN_t \rightarrow \sigma^*C_1$–$C_2$	37	35	35	35	34	34	33	33	33	33
$LpN_t \rightarrow \sigma^*C_1$–H[d]	5/5	4/4	4/4	4/4	4/4	4/4	4/4	4/4	4/4	4/4
$LpN_c \rightarrow \sigma^*$ C_3–H	36	35	34	34	34	33	33	33	33	33
$LpN_c \rightarrow \sigma^*C_{3'}$–H	36	35	34	34	34	33	33	33	33	33
$LpN_c \rightarrow \sigma^*N_t$–H	—	—	—	—	—	—	—	—	—	—
$LpN_t' \rightarrow \sigma^*C_1'$–$C_2'$	37	35	35	35	34	34	33	33	33	33
$LpN_t' \rightarrow \sigma^*C_1'$–H[d]	5/5	4/4	4/4	4/4	4/4	4/4	4/4	4/4	4/4	4/4
$LpN_t' \rightarrow \sigma^*N_c$–H	—	—	—	—	—	—	—	—	—	—
Dipole moment										
Net	1.50	1.74	1.83	1.85	1.95	2.12	2.25	2.27	2.29	2.31
Delocalization correction	0.78	0.79	0.80	0.80	0.81	0.82	0.84	0.84	0.84	0.85
Total	1.87	2.17	2.28	2.31	2.43	2.63	2.79	2.82	2.84	2.86
Second-order stabilization energies[c]					*tGG′Tg′TG′Gg′*					
$LpN_t \rightarrow \sigma^*C_1$–$C_2$	38	37	36	36	36	36	35	35	35	35
$LpN_c \rightarrow \sigma^*$ C_3–H	34/5	33/5	32/5	32/5	32/5	32/5	31/5	31/5	31/5	31/5
$LpN_c \rightarrow \sigma^*C_3'$–H	36/7	35/6	34/6	34/6	34/6	33/6	33/5	33/5	33/5	33/5
$LpN_c \rightarrow \sigma^*N_t$–H	24	22	21	21	20	18	16	16	16	16
$LpN_t' \rightarrow \sigma^*C_1'$–H	31/3	31/3	31/3	31/3	31/3	30/3	30/3	30/3	30/3	30/3
$LpN_t' \rightarrow \sigma^*C_1'$–$C_2'$	5	4	4	4	4	4	4	4	4	3
$LpN_t' \rightarrow \sigma^*N_c$–H	33	21	20	20	19	18	17	17	17	17
Dipole moment										
Net	3.89	4.12	4.20	4.21	4.29	4.40	4.47	4.47	4.48	4.49
Delocalization correction	1.00	0.93	0.91	0.91	0.91	0.90	0.89	0.89	0.89	0.89
Total	3.72	3.99	4.09	4.11	4.20	4.34	4.42	4.43	4.45	4.45
Wiberg index										
(N_t–)H⋯N_c	0.0235	0.0234	0.0230	0.0229	0.0222	0.0210	0.0203	0.0203	0.0202	0.0201
(N_c–)H⋯N_t'	0.0275	0.0212	0.0205	0.0205	0.0203	0.0201	0.0200	0.0199	0.0199	0.0199

Lp and σ* stand for lone pair and antibonding sigma orbital, respectively.
[a] N_t and N_t' stand for terminal nitrogen atoms that act as donor and acceptor, respectively in the *tGG′Tg′TG′Gg′* conformer (Fig. S1); for conformer *tTTTg′TTTt* they are equivalent.
[b] Critical ε-value.
[c] In kJ mol^{-1}.
[d] The two H-atoms linked to C-atom.

partially explain the stability increase predicted for conformer tTTT-TTTt, relative to conformer tGG′T-TG′Gg′, as dielectric constant increases.

3.1.1. Intermolecular hydrogen bonding effects

In the condensed pure liquid phase, the likelihood of establishing intermolecular contacts is very high. In the case of amines, the NH_2 and NH groups are particularly prone to the establishment of intermolecular N–H···N hydrogen bonds. The relevance of these stabilizing interactions on the overall stability most likely overwhelms that of potential intramolecular interactions. In the case of NSpd, this would translate into a relative stability increase of the almost-fully *trans* conformation (tTTT-TTTt) which, in the limit, would become the more stable conformer. Therefore, it is important to evaluate the influence of the potential intermolecular N–H···N contacts on the forecasts of the NSpd vibrational frequencies.

In order to evaluate the preferences of the NH_2 and NH groups of NSpd for establishing intermolecular hydrogen bonding, six distinct molecular adduct models, based on the tTTT-TTTt conformation, were assembled and fully optimized. In all those models, the NSpd partners in the hydrogen bonding are ammonia molecules, in order to maintain the computational demands low. In the two smallest adduct models, each terminal NH_2–group is involved in two N–H···N interactions, with two distinct NH_3 molecules, acting simultaneously as donors and acceptors (**d–a** H-bond profile), while the central NH group is involved in one N–H···N interaction, acting either as a donor (**model 1**) or as an acceptor (**model 2**). All the attempts made to optimize adducts with the terminal NH_2-group acting as double donors (**d–d** H-bond profile) failed, always converging to a **d–a** H-bond profile. This inability to optimize the **d–d** H-bond profile evidences the preference of the NH_2 groups for a **d–a** arrangement, in line with the results previously reported for iPram [28].

Model 3 differs from the preceding insofar as the central NH group also presents a **d–a** H-bonding profile. In the next two models, the hydrogen bonding capacities of the NH_2 groups are fully satisfied (**d–a–d** H-bond profile), wherein the NH group acts either as acceptor (**model 4**) or donor (**model 5**). Finally, in the larger adduct model (**model 6**), the maximum H-bonding capacities of both NH_2 and NH groups are completely contemplated. Fig. 4 presents the optimized geometries determined all six NSpd·NH_3 adduct models, along with the distances characterizing the N–H···N intermolecular interactions established.

In view of getting insights on the stabilizing effects of the distinct hydrogen bonding patterns considered, two energetic parameters were

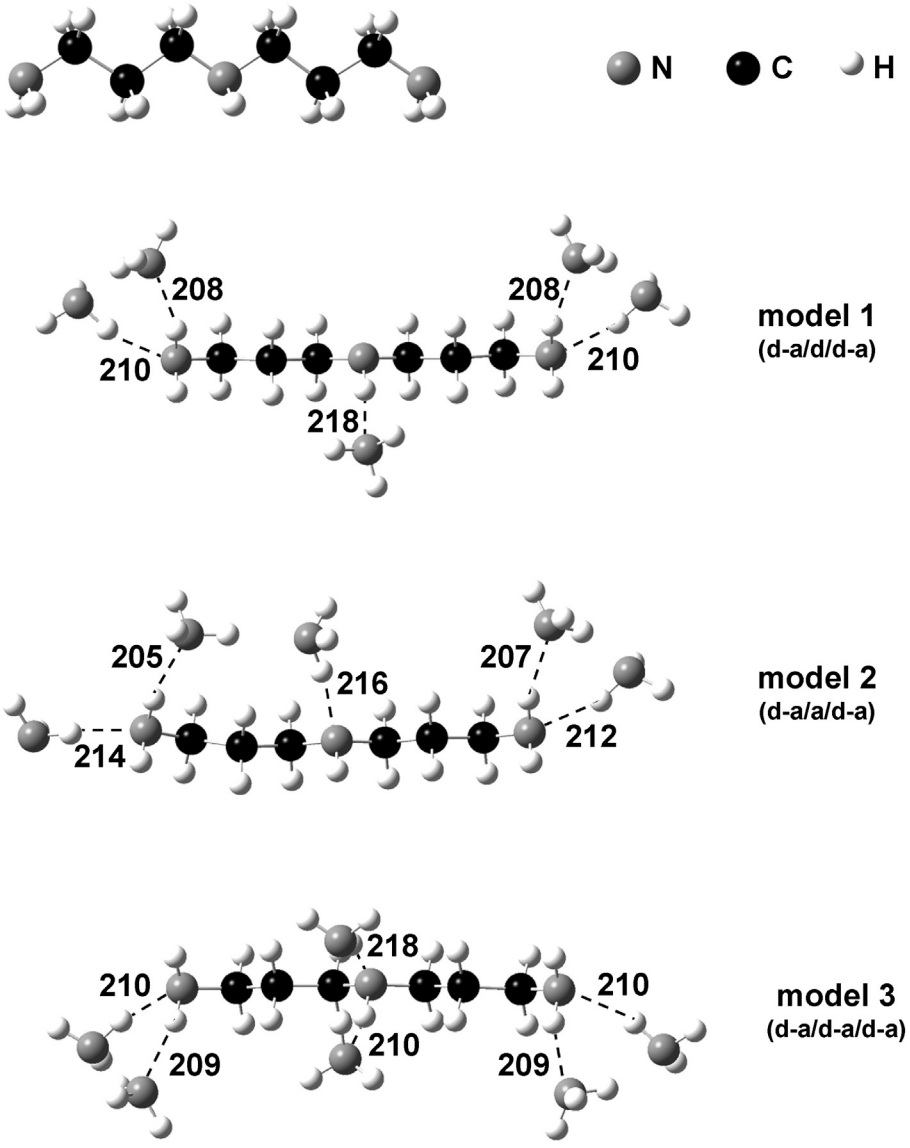

Fig. 4. Optimized geometries achieved for the six molecular NSpd–NH_2 adducts simulating all potential hydrogen bonding acceptor/donor patterns possible for the NSpd NH_2 and NH groups. The H-bond distances between NSpd and surrounding NH_3 molecules are indicated (in pm).

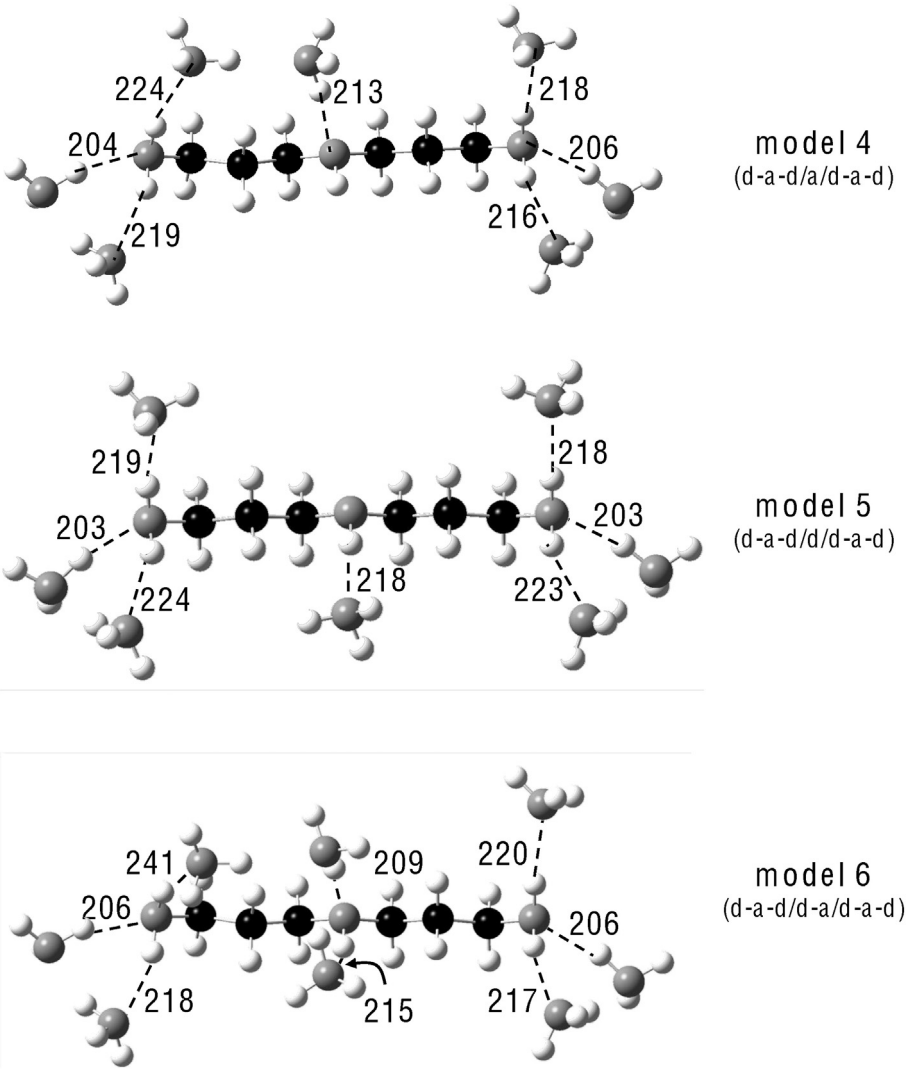

Fig. 4 (*continued*).

evaluated, namely the adduct formation energy (ΔE_{adduct}) and the cooperativity effect between multiple H-bonds (CEHB). These energetic parameters were quantified as previously for iPram [28], using expressions (1) and (2), respectively

$$\Delta E_{adduct} = -[E_{adduct} - (E_{NSpd} + n \times E_{NH_3})] \quad (1)$$

$$CEHB_{adduct} = \Delta E_{adduct} - ((i \times \Delta E_{(NH_2)_d} + j \times \Delta E_{(NH_2)_a} + k \times \Delta E_{(NH)_d} + l \times \Delta E_{(NH)_a}), \quad (2)$$

where **n** stands for the number of NH_3 molecules of the adduct, **i** and **j** stand for the number of times the terminal NH_2 groups act as donor and acceptor, respectively, and **k** and **l** stand for the number of times the central NH group acts as donor or acceptor, respectively. The values of $\Delta E_{(NH_2)d}$, $\Delta E_{(NH_2)a}$, $\Delta E_{(NH)d}$ and $\Delta E_{(NH)a}$ were determined following Eq. (1), considering the energies obtained in the calculations performed for adducts presenting a NSpd–to–NH_3 stoichiometry of 1:1 with the H-bond style indicated in subscript (involving either the NH_2 or the NH group, as acceptor, **a**, or as donor, **d**).

According to the calculations performed for the 1:1 NSpd–to–NH_3 adducts, a donor involvement of the NH_2 groups provides a greater adduct stability by *ca.* 1.2 kJ mol^{-1}, with respect to the acceptor involvement. Regarding the NH group, no preference is highlighted, the predicted energy difference between the two types of adducts ($\Delta E_{(NH)d}$ *vs.* $\Delta E_{(NH)a}$) being less than 0.05 kJ mol^{-1}. This independence of the NH group with regard to the type of participation in hydrogen bonding does not stand when the more complex adduct models are considered (Fig. 4).

Fig. 5 shows the variation of both ΔE_{adduct} and CEHB parameters as a function of adduct model (Fig. 4). Opposing to what was observed for the 1:1 adducts, the preference of the NH group for an acceptor H-

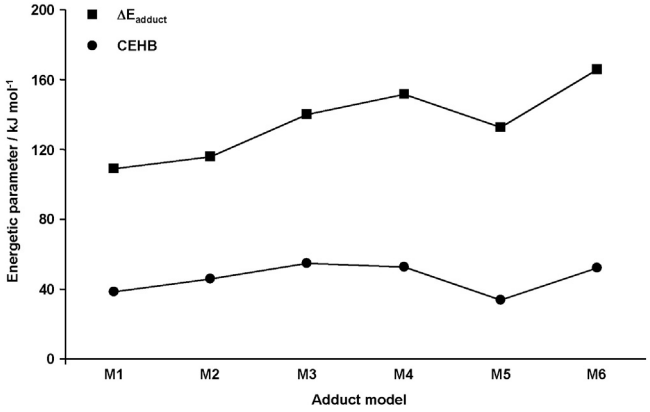

Fig. 5. Variation of the ΔE_{adduct} and CEHB values as a function of adduct model (for definition of the ΔE_{adduct} and CEHB values see text).

bond involvement is evident. This stands regardless of whether the maximum engagement capacities of the terminal NH_2 groups are fulfilled or not. Comparing the ΔE_{adduct} values determined for the two smaller adduct models, the acceptor involvement of the NH group (model 2) is predicted to be stabilized by more than 7 kJ mol^{-1} with respect to a donor-type participation (model 1). This stabilization effect of the NH acceptor-like involvement is significantly accentuated when the hydrogen bonding capacities of the terminal NH_2 are fulfilled (model 4 *vs.* model 5).

Usually, increasing the number of molecules within the adducts is expected to increase ΔE_{adduct} [28,43,44]. This general rule is observed in the present work with only one exception, when passing from adduct model 3 to adduct model 5, in which case, the calculations predict a ΔE_{adduct} reduction of about 13 kJ mol^{-1}. This result evidences a destabilizing effect of the NH involvement as a donor, thus emphasizing the preference of the of an acceptor-like involvement.

Fulfilling the hydrogen bonding capacity of both primary and secondary amine groups (model 6) increases the adduct formation energy (116 kJ mol^{-1} in model 2 *vs.* 166 kJ mol^{-1} in model 6). However, this effect is clearly not due to an enhancement of the positive cooperative effect between the multiple H-bonds. As seen in Fig. 5, a maximum CEHB is achieved in adduct model 3. Passing from adduct model 3 (CEHB = 55 kJ mol^{-1}) to adduct models 4 to 6 leads to CEHB drops of 3, 21 and 3 kJ mol^{-1}, respectively. This means that maximum positive H-bond cooperativity in NSpd is expected if two premises are met: (i) the H-bonding capacity of the NH group is fulfilled (**d–a** pattern) and (ii) the NH_2 H-bond involvement is also a **d–a** pattern (*i.e.*, H-bond involvement capacity not fully satisfied). Te later is in accordance with the results previously reported for the hydrogen bonding preferences of the NH_2 group in iPram [28].

3.2. Vibrational analysis

NSpd presents a total of 72 vibrational modes. The 13 lowest frequency vibrations correspond to the skeletal deformations, namely 7 longitudinal and 6 transversal acoustic modes (LAMs and TAMs, respectively). The assignment of these low frequency vibrations exclusively based on the Raman spectra can be rather arguable, their identification being more surest using the complementary INS technique [17,19]. Moreover, these low-frequency vibrational modes are highly overlapped by the lattice vibrations in the molecular adducts. Therefore, they are not addressed in the present study.

The remaining 59 vibrational modes correspond to 25 stretchings (4 νNH_2, 12 νCH_2, 1 νNH, 2 $\nu C–NH_2$, 2 $\nu C–NH$ and 4 $\nu C–C$), 8 scissorings (2 δNH_2 and 6 δCH_2), 8 waggings (2 ωNH_2 and 6 ωCH_2), 8 twistings (2 tNH_2 and 6 tCH_2) and 8 rockings (2 ρNH_2 and 6 ρCH_2), and 1 in-plane and 1 out-of-plane N–H deformations (βNH and γNH, respectively).

The effects of the involvement of amine groups in hydrogen bonding on the predictions of the corresponding vibrational frequencies have been extensively assessed, both experimentally and theoretically [18,28,33,45–48]. A recent quantum chemical study performed on iPram [28], for instance, showed that the NH_2 involvement in intermolecular N–H···N interactions has a pronounced effect on the NH_2 stretching, wagging and rocking modes. The remaining vibrational modes were found to be comparatively much less affected, with those ascribed to the CH_2-groups remaining almost unaffected. Concordant results were recently reported regarding the effects of the interactions with counterions on the vibrational frequencies of α,ω-diamines hydrochloride salts [33].

Table 2 presents and compares the non-scaled vibrational frequencies calculated for NSpd in the isolated form and within the six molecular adducts tested. The deviations promoted by the distinct hydrogen bonding patterns on each NSpd vibrational mode, relative to the isolated state ($\Delta = \omega_{adduct} - \omega_{NSpd}$), are also presented. Assignments were made on the basis of the atomic displacements predicted and visualized using the GaussView program package [49].

In line with other reported works [18,28,33,50,51], the effects of the intermolecular N–H···N interactions are particularly noticed on the $\nu_s NH_2$, $\nu_{as} NH_2$, ωNH_2, ρNH_2, νNH and γNH. While the stretching modes ($\nu_s NH_2$, $\nu_{as} NH_2$ and νNH) are pronouncedly red-shifted, all remaining modes are blue-shifted. The magnitude of the deviations is clearly dependent on the degree (number of established interactions) and type (acceptor *vs.* donor) of participation of the NH and NH_2 groups within the overall hydrogen bonding network.

Regarding the H-bonding of the central NH group, its involvement as an acceptor was found to have a relatively small effect on any of the three related vibrational modes, νNH, βNH and γNH (isolated NSpd *vs.* adduct models 2 and 4). In contrast, its donor-like involvement leads to significant downward and upward shifts of the νNH and γNH modes, respectively. The effect of cooperativity between the hydrogen bonds involving the NH group and the hydrogen bonds involving the NH_2 groups seems to be negligible. In fact, the deviations predicted for the νNH and γNH modes for the 1:1 NSpd·NH_3 molecular adduct (presenting the NH group involved in a H-bond with NH_3 as a donor; not shown) are of the same magnitude as those predicted for adduct models 1 and 5 (νNH: -92 cm^{-1} *vs.* -90 cm^{-1} (model 1) and -94 cm^{-1} (model 5); γNH: 132 cm^{-1} *vs.* 127 cm^{-1} (model 1) and 139 cm^{-1} (model 5)). However, the same is not observed when the effect of cooperativity between two hydrogen bonds centred at the NH group (**d–a** profile) is evaluated. In this case, H-bonding cooperativity enhances the frequency deviations, as evidenced by the change of model 1 to model 3 or of model 5 to model 6. Interestingly, the maximum effect of H-bonding cooperativity on the magnitude of the deviations is observed when model 1 is transformed into model 3, which corresponds to the adduct model displaying the highest CEHB value.

Considering the NH_2 most affected vibrational modes ($\nu_s NH_2$, $\nu_{as} NH_2$, ωNH_2 and ρNH_2), the calculations performed for the 1:1 NSpd·NH_3 molecular adduct presenting the NH_2 group engaged in the H-bond to the NH_3 molecule (results not shown) suggest that, as for the NH vibrations, acceptor involvement has in general a very smooth effect. The only exception is observed for the ρNH_2 mode, for which an acceptor-like involvement of the NH_2 group leads to a blue-shift of 192 cm^{-1}. On the other hand, the donor involvement of the NH_2 group in a 1:1 NSpd·NH_3 molecular adduct leads to slightly larger deviations, though only the ρNH_2 mode is shifted by more than 100 cm^{-1} (results not shown).

Enhancing the NH_2 participation in the H-bonding pattern, while keeping the NH involvement (1:1 → model 1 → model 5 or 1:1 → model 2 → model 4), progressively accentuates the deviation of the $\nu_{as} NH_2$, ωNH_2 and ρNH_2. The $\nu_s NH_2$, in turn, shows pronounced deviation that increases when going from adduct 1:1 to either models 1 or 2, but evidence the opposite when comparing models 1 and 2 with models 4 and 5, respectively. Fulfilling the hydrogen bonding capacity of the NH group (model 5 → model 6) does not change the variation trends described.

In short, the results currently presented reinforce the idea, vastly reported in the literature, intermolecular interactions, as hydrogen bonding, may significantly affect the spectral position of certain vibrational modes. Therefore, it is extremely important that those effects are taken into account when allocating experimentally observed spectral features based on the theoretical spectral forecasts. Therefore, the next section presents a reassessment of the vibrational assignments already reported in the literature, given that the energy assessment made in this work pointed adduct model 3 as ensuring a higher overall stability, judging by the greater H-bonding cooperativity predicted (larger CEHB value).

3.2.1. Assignment of the experimental vibrational spectra

Fig. 6 shows the vibrational spectra (FT-Raman and FTIR) of pure liquid NSpd, in the 100–1750 cm^{-1} and 2250–3750 cm^{-1} spectral regions. Table 3 presents the vibrational assignments for NSpd, based on the

Table 2
Non-scaled vibrational frequencies calculated for NSpd considering the isolated molecule and the six molecular adducts tested for each vibrational mode the forecasted deviations upon formation of the N–H···N interactions that hold the adduct structure are presented. The assignments made are based on the atomic displacements predicted and visualized using the GaussView program [49].

NSpd	Molecular adducts[a]												Vibrational assignment[d]
	Model 1		Model 2		Model 3		Model 4		Model 5		Model 6		
	ω[b]	Δ[c]	ω[b]	Δ[c]	ω[b]	Δ[c]	ω[b]	Δ[c]	ω[b]	Δ[c]	ω[b]	Δ[c]	
3599	3554	−45	3555	−44	3554	−45	3480	−119	3488	−111	3490	−109	ν_{as} NH_2
3599	3552	−47	3555	−44	3554	−45	3472	−127	3486	−113	3487	−112	
3509	3387	−122	3372	−137	3376	−133	3394	−115	3406	−103	3400	−109	ν_{s} NH_2
3509	3378	−131	3315	−194	3376	−133	3390	−119	3404	−105	3399	−110	
1713	1747	34	1748	35	1746	33	1762	49	1761	48	1762	49	δ NH_2
1713	1746	33	1732	19	1746	33	1754	41	1761	48	1758	45	
898	1000	102	1005	107	1023	125	1030	132	1024	126	1028	130	ω NH_2
896	992	96	993	97	998	102	1007	111	1014	118	1020	124	
1055	1078	23	1074	19	1066	11	1090	35	1093	38	1091	36	t NH_2
1035	1056	21	1045	10	1054	19	1056	21	1076	41	1075	40	
306	629	323	650	344	628	322	693	387	681	375	684	378	ρ NH_2
306	626	320	630	324	626	320	687	381	678	372	661	355	
3520	3430	−90	3519	−1	3349	−171	3515	−5	3426	−94	3402	−118	ν NH
1524	1592	68	1514	−10	1601	77	1514	−10	1592	68	1583	59	β NH
809	936	127	833	24	980	171	846	37	948	139	971	162	γ NH
3120	3119	−1	3138	18	3118	−2	3145	15	3116	−4	3137	17	ν_{as} CH_2
3120	3117	−3	3116	−4	3117	−3	3114	−6	3114	−6	3114	−6	
3095	3093	−2	3096	1	3092	−3	3090	−5	3083	−12	3092	−3	
3095	3091	−4	3091	−4	3092	−3	3084	−11	3081	−14	3081	−14	
3077	3064	−13	3076	−1	3056	−21	3075	−2	3063	−14	3055	−22	
3074	3059	−15	3074	0	3055	−19	3073	−1	3061	−13	3052	−22	
3067	3055	−12	3060	−7	3062	−5	3055	−12	3049	−18	3070	3	ν_{s} CH_2
3067	3053	−14	3054	−13	3061	−6	3053	−14	3048	−19	3063	−4	
3040	3051	11	3051	11	3053	13	3047	7	3046	6	3050	10	
3040	3044	4	3045	5	3052	12	3047	7	3045	5	3045	5	
2952	2927	−25	2975	23	2953	1	2975	23	2925	−27	2966	14	
2947	2920	−27	2968	21	2946	1	2968	21	2919	−28	2955	8	
1559	1559	0	1558	−1	1557	−2	1558	−1	1559	0	1558	−1	δ CH_2
1547	1546	−1	1547	0	1545	−2	1547	0	1546	−1	1547	0	
1532	1533	1	1532	0	1532	0	1532	0	1532	0	1534	2	
1530	1530	0	1530	0	1529	−1	1530	0	1530	0	1530	0	
1518	1520	2	1521	3	1519	1	1521	3	1519	1	1522	4	
1517	1519	2	1519	2	1518	1	1519	2	1518	1	1519	2	
1458	1457	−1	1455	−3	1456	−2	1452	−6	1454	−4	1453	−5	ω CH_2
1431	1428	−3	1430	−1	1427	−4	1430	−1	1427	−4	1430	−1	
1418	1415	−3	1417	−1	1414	−4	1417	−1	1414	−4	1414	−4	
1396	1397	1	1394	−2	1398	2	1392	−4	1396	0	1393	−3	
1311	1311	0	1326	15	1314	3	1319	8	1310	−1	1321	10	
1284	1287	3	1288	4	1291	7	1292	8	1287	3	1292	8	
1418	1437	19	1449	31	1437	19	1463	45	1453	5	1454	36	t CH_2
1417	1434	17	1440	23	1434	17	1458	41	1452	35	1450	33	
1347	1344	−3	1354	7	1345	−2	1353	6	1344	−3	1349	2	
1341	1340	−1	1348	7	1341	0	1345	4	1340	−1	1323	−18	
1336	1339	3	1341	5	1340	4	1341	5	1338	2	1335	−1	
1308	1315	7	1313	5	1313	5	1315	7	1315	7	1312	4	
1253	1267	14	1257	4	1278	25	1252	−1	1275	22	1251	−2	ρ CH_2
1159	1169	10	1166	7	1167	8	1173	14	1172	13	1174	15	
879	874	−5	890	11	875	−4	899	20	878	−1	887	8	
854	860	6	863	9	859	5	867	13	865	11	869	15	
762	766	4	765	3	764	2	766	4	764	2	767	5	
761	764	3	762	1	761	0	762	1	762	1	764	3	
1193	1200	7	1182	−11	1190	−3	1184	−9	1198	5	1188	−5	ν_{as} C–NH
1035	1090	55	1125	90	1092	57	1074	39	1076	41	1074	39	ν_{s} C–NH
1133	1152	19	1154	21	1154	21	1127	−6	1127	−6	1128	−5	ν C–NH_2
1119	1122	3	1099	−20	1132	13	1102	−17	1099	−20	1100	−19	
1170	1185	15	1194	24	1181	11	1199	29	1193	23	1198	28	ν C–C
1087	1100	13	1094	7	1103	16	1160	73	1161	74	1164	77	
1081	1094	13	1083	2	1099	18	1097	16	1098	17	1103	22	
1054	1053	−1	1054	0	1055	1	1075	21	1058	4	1060	6	

[a] In accord to Fig. 2.
[b] Non-scaled theoretical vibrational frequency.
[c] Shifts promoted on the NSpd vibrational modes upon adduct formation ($\Delta_i = \omega_i(adduct) - \omega_i(NSpd)$).
[d] ν = stretching, δ = scissoring, ω = wagging, ρ = rocking, t = twisting, β = in-plane deformation and γ = out-of-plane deformation; **as** and **s** stand for asymmetric and symmetric, respectively.

vibrational frequency calculations performed in this work. The calculated theoretical frequencies were corrected for anharmonicity and incomplete electron correlation treatment, by using the scaling factor of 0.9499 proposed by Merrick et al. [52] for the mPW1PW/6-31G* theory level. Moreover, as stated above, the account for the effects of hydrogen bonding was accounted for by considering adduct model 3 (Fig. 4). For the reasons already pointed, the LAM and TAM vibrational modes are not discriminated.

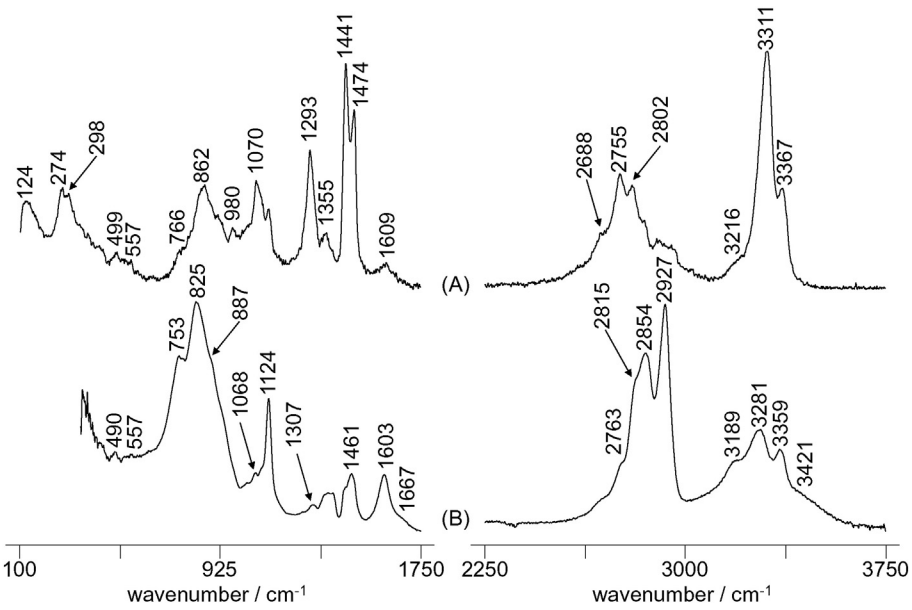

Fig. 6. Experimental vibrational spectra of NSpd in the 100–1750 cm^{-1} and 2250–3750 cm^{-1} spectral regions: (A) FT-Raman and (B) FTIR.

On the whole, the assignments performed are in good agreement with the standard assignments gathered in the literature for this kind of systems [50,53–55]. The $\nu_{as}NH_2$ are significantly blue-shifted relatively to the ν_sNH_2, while the νNH is predicted to be mixed with these later. A shoulder observed around 3200 cm^{-1} has been appointed as a fingerprint of primary amines, being to an overtone of the δNH_2 mode observed at *ca.* 1600 cm^{-1} [53,55]. Therefore, it is reasonably to ascribe the shoulder observed at 3189 cm^{-1} in the FTIR spectrum (Fig. 6) to an overtone of the δNH_2 mode ascribed to the spectral feature at 1603 cm^{-1}.

Three vibrational modes that deserve a special reference are the tNH_2, the ωNH_2 and the γNH modes. Benchmark literature [50,53–55] point tNH_2, the ωNH_2 and the γNH modes as being highly mixed within the 850–700 cm^{-1} spectral region. The calculations performed on adduct model 3 confirm the marked mixing between the ωNH_2 and γNH modes. These vibrational modes are referred to as giving rise to intense and broad bands [50,53,55]. Ascribing the spectral features observed at 825 and 862 cm^{-1} to a mixture of both ωNH_2 and γNH modes is in line with the information available in the literature. With respect to the γNH mode the data available positioning it around 740 cm^{-1} [40,41,56], *i.e.*, at a significantly lower frequency than proposed herein. This is most likely related to more significant hydrogen bonding effects in NSpd, which is a triamine, compared to the monoamines regarded in those reports.

With regard to tNH_2 modes, the calculations predict them at higher frequency values than the ωNH_2 and γNH modes, turning them mixed with the skeleton elongation modes νC–C and ν_sC–NH. These trends are also observed considering the calculations performed for the isolated NSpd molecule.

The ρNH_2 are, beyond doubt, the NSpd vibrational modes whose behaviour as a result of the NH_2 involvement in hydrogen bonds are worth to be scrutinized. Unfortunately, the ρNH_2 modes give rise to very weak spectral features in both Raman and occur mid-IR spectra.

Calculations on the isolated NSpd molecule predict the ρNH_2 modes at 306 cm^{-1}. Accounting for the effects of N–H···N interactions leads to a significant blue-shifting of the ρNH_2 vibrations, placing them at 597 cm^{-1} after scaling. Such an effect has been widely reported in the literature for systems containing amine groups involved in strong intermolecular N–H···N interactions [18,28,51]. Based on the proximity principle, we ascribe the ρNH_2 vibrational modes to the weak Raman feature around 557 cm^{-1}. A more reliable allocation would be achieved using INS. The INS studies performed on several di- and triamines, for example, allocate the ρNH_2 vibrational modes in the spectral region 530–550 cm^{-1} [17], in agreement with the assignment herein proposed.

4. Conclusions

The present study presents a thorough conformational study on NSpd. The most stable conformation in the condensed phase was inferred based on SCRF calculations and discussed on the light of the conformational preferences predicted for the isolated state (gas-phase). The study culminates with a full assignment of the NSpd vibrational spectra, which reassessment justifies as the prior report [23] besides being incomplete presents outstanding inconsistencies.

On the whole, it was found that the most stable conformation in the gas-phase corresponds to the tGG′T-TG′Gg′ geometry, which is stabilized by two intramolecular N–H···N hydrogen bonds. The overall stabilizing relevance of the two H-bonds does not seem to be the same, judging by the distances H···N that characterize them. In addition, they are affected differently by the dielectric constant.

Assuming that in the condensed phase the stabilizing effect of intermolecular N–H···N hydrogen bonds eventually overwhelm those of the intramolecular N–H···N ones, distinct NSpd-NH_3 adducts were simulated in order to evaluate the relevance of considering different hydrogen bonding patterns on the overall stability and on the vibrational frequencies of NSpd. It was found that the highest CEHB is achieved by considering an adduct presenting all three amine groups engaged in two H-bonds to distinct NH_3 molecules, in all cases with an overall **d–a** pattern (model 3). This result was used to infer the effects of hydrogen bonding on the relative positioning of the NSpd vibrational modes. Special attention was given to the νNH_2, ωNH_2, ρNH_2, νNH and γNH modes as they are particularly affected.

To finalize only a word of precaution, the present report clearly evidences that an accurate prediction of the vibrational frequencies requires at the outset a correct description of the molecular entity being studied. Otherwise, an incorrect description of the molecular structure and/or electronic distribution will lead to erroneous forecasts of the vibrational frequencies, culminating in inaccurate assignments.

Supplementary data to this article can be found online at http://dx.doi.org/10.1016/j.saa.2016.01.003.

Table 3
Assignment of the vibrational spectra (Raman and FTIR) of pure liquid NSpd.

Experimental		Isolated NSpd		Model 3		Assignment[c]
Raman	FTIR	ω[a]	scal.[b]	ω[a]	scal.[b]	
3367	3359	3599	3419	3554	3376	$\nu_{as}NH_2$
3311		3599	3419	3554	3376	
	3281	3509	3333	3376	3207	$\nu_{s}NH_2$
		3509	3333	3207	3046	
3216		3520	3344	3349	3181	νNH
	3189					FR ($2x\delta NH_2$)
2957		3120	2964	3118	2962	$\nu_{as}CH_2$
		3120	2964	3117	2961	
	2927	3095	2940	3092	2937	
		3095	2940	3092	2937	
2900		3067	2913	3062	2909	$\nu_{s}CH_2$
		3067	2913	3061	2908	
2849	2854	3077	2923	3056	2903	$\nu_{as}CH_2$
		3074	2920	3055	2902	
		3040	2888	3053	2900	$\nu_{s}CH_2$
		3040	2888	3052	2899	
2802	2815	2952	2804	2953	2805	
2755	2763	2947	2799	2946	2798	
2688	2689					
	1667					
1609	1603	1713	1627	1746	1659	δNH_2
		1713	1627	1746	1659	
		1524	1448	1601	1521	βNH
1474		1559	1481	1557	1479	δCH_2
	1461	1547	1469	1545	1468	
1441	1440	1532	1455	1532	1455	
		1530	1453	1529	1452	
	1389	1518	1442	1519	1443	
		1517	1441	1518	1442	
		1458	1385	1456	1383	ωCH_2
	1369	1418	1347	1437	1365	tCH_2
		1418	1347	1434	1362	
1355	1353	1431	1359	1427	1356	ωCH_2
		1417	1346	1414	1343	
		1396	1326	1398	1328	
	1307	1347	1280	1345	1278	tCH_2
		1341	1274	1341	1274	
		1336	1269	1340	1273	
1293		1311	1245	1314	1248	ωCH_2
		1308	1242	1313	1247	tCH_2
		1284	1220	1291	1226	ωCH_2
		1253	1190	1278	1214	ρCH_2
1122	1124	1193	1133	1190	1130	$\nu_{as}C–NH$
		1170	1111	1181	1122	νC–C
		1159	1101	1167	1109	ρCH_2
	1095	1133	1076	1154	1096	$\nu C–NH_2$
1070	1068	1119	1063	1132	1075	
1044	1037	1087	1033	1103	1048	νC–C
		1081	1027	1099	1044	νC–C
		1035	983	1092	1037	$\nu_{s}C–NH$
980		1055	1002	1066	1013	tNH_2
915		1054	1001	1055	1002	
		1035	983	1054	1001	νC–C
862		898	853	1023	972	ωNH_2
		896	851	998	948	
	825	809	768	980	931	γNH
764	753	879	835	875	831	ρCH_2
		854	811	859	816	
		762	724	764	726	
		761	723	761	723	
557		306[d]		628	597	ρNH_2
		306[d]		628	597	

[a] Calculated frequency value.
[b] Scaled values in accord to Merrick et al. [52] (λ = 0.9499).
[c] ν = stretching, δ = scissoring, ω = wagging, ρ = rocking, t = twisting, β = in-plane deformation and γ = out-of-plane deformation; **as** and **s** stand for asymmetric and symmetric, respectively.
[d] Not scaled as suggested by Merrick et al. [52].

Acknowledgements

The authors acknowledge financial support from the Portuguese Foundation for Science and Technology — Unidade de Química-Física Molecular (UID/Multi/00070/2013). TMS also acknowledges the Portuguese Foundation for Science and Technology for a PhD fellowship (SFRH/BD/46364/2008). Acknowledgements are also due to Laboratório Associado CICECO, University of Aveiro, Portugal, for the free access to the FTIR-ATR and FT-Raman spectrometers and computational facilities (G09w program).

References

[1] N. Umezawa, Y. Horai, Y. Imamura, M. Kawakubo, M. Nakahira, N. Kato, A. Muramatsu, Y. Yoshikawa, K. Yoshikawa, T. Higuchi, Structurally diverse polyamines: solid-phase synthesis and interaction with DNA, Chembiochem 16 (2015) 1811–1819.
[2] W. Pan, J. Zhou, Y. Yin, H. Wen, D. Liang, Local de-condensation of double-stranded DNA in oppositely charged polyelectrolyte as induced by spermidine, Soft Matter 11 (2015) 4705–4709.
[3] T.L. Mastracci, M.A. Robertson, R.G. Mirmira, R.M. Anderson, Polyamine biosynthesis is critical for growth and differentiation of the pancreas, Scientific Reports 5 (2015), 13269.
[4] P. Icard, T. Vallantin, P. Kafara, J.M. Steyaert, L. Schwartz, H. Lincet, The decrease of citrate in tumor cells: a gauge to upgrade? Oncologie 17 (2015) 315–320.
[5] T.M. Silva, H. Cirenajwis, H.M. Wallace, S. Oredsson, L. Persson, A role for antizyme inhibitor in cell proliferation, Amino Acids 47 (2015) 1341–1352.
[6] W. Huang, J.C. Eickhoff, F. Mehraein-Ghomi, D.R. Church, G. Wilding, H.S. Basu, Expression of spermidine/spermine N-1-acetyl transferase (SSAT) in human prostate tissues is related to prostate cancer progression and metastasis, Prostate 75 (2015) 1150–1159.
[7] L.Y. Cho, J.J. Yang, K.-P. Ko, S.H. Ma, A. Shin, B.Y. Choi, H.J. Kim, D.S. Han, K.S. Song, Y.S. Kim, S.-H. Chang, H.-R. Shin, D. Kang, K.-Y. Yoo, S.K. Park, Gene polymorphisms in the ornithine decarboxylase-polyamine pathway modify gastric cancer risk by interaction with isoflavone concentrations, Gastric Cancer 18 (2015) 495–503.
[8] L. Xu, J. Long, P. Wang, K. Liu, L. Mai, Y. Guo, Association between the ornithine decarboxylase G316A polymorphism and breast, Oncol. Lett. 10 (2015) 485–491.
[9] E. Agostinelli, C. Barrero, E. Bidollari, S. Ohkubo, M. Xhani, A. Toninello, S. Merali, Can polyamines be used to combat cancer? New therapeutic approaches, Amino Acids 47 (2015) 1664.
[10] B. Lorgulescu, S. Patel, J. Louro, C. Andrade, A. Sanchez, D. Pearse, 182Acute putrescine supplementation with Schwann cell transplantation improves sensory and serotonergic axon growth and functional recovery in spinal cord injury, Neurosurgery 62 (2015) 226–227.
[11] N. Han, L. Yu, Z. Song, L. Luo, Y. Wu, Agmatine protects Muller cells from high-concentration glucose-induced cell damage via N-methyl-D-aspartic acid receptor inhibition, Mol. Med. Rep. 12 (2015) 1098–1106.
[12] B. Rosenberg, L.V. Camp, T. Krigas, Inhibition of cell division in *Escherichia coli* by electrolysis products from a platinum electrode, Nature 205 (1965) 698–699.
[13] B. Rosenberg, L. Vancamp, J.E. Trosko, V.H. Mansour, Platinum compounds — a new class of potent antitumour agents, Nature 222 (1969) 385–387.
[14] B. Rosenberg, Some biological effects of platinum compounds — new agents for the control of tumours, Platin. Met. Rev. 15 (1971) 42–51.
[15] M.J. Cleare, J.D. Hoeschele, Anti-tumour platinum compounds — relationship between structure and activity, Platin. Met. Rev. 17 (1973) 2–13.
[16] K. Wang, E. Gao, Recent advances in multinuclear complexes as potential anticancer and DNA binding agents, Anti Cancer Agents Med. Chem. 14 (2014) 147–169.
[17] M.P.M. Marques, L.A.E. Batista de Carvalho, J. Tomkinson, Study of biogenic and α,ω-polyamines by combined inelastic neutron scattering and Raman spectroscopies and by ab initio molecular orbital calculations, J. Phys. Chem. A 106 (2002) 2473–2482.
[18] A.M. Amado, J.C. Otero, M.P.M. Marques, L.A.E. Batista de Carvalho, Spectroscopic and theoretical studies on solid 1,2-ethylenediamine dihydrochloride salt, ChemPhysChem 5 (2004) 1837–1847.
[19] L.A.E. Batista de Carvalho, M.P.M. Marques, J. Tomkinson, Transverse acoustic modes of biogenic and α,ω-polyamines: a study by inelastic neutron scattering and Raman spectroscopies coupled to DFT calculations, J. Phys. Chem. A 110 (2006) 12947–12954.
[20] A.M. Amado, S.M. Fiuza, M.P.M. Marques, L.A.E. Batista de Carvalho, Conformational and vibrational study of platinum(II) anticancer drugs: cis-diamminedichloroplatinum(II) as a case study, J. Chem. Phys. 127 (2007), 185104.
[21] M.P.M. Marques, L.A.E. Batista de Carvalho, Vibrational spectroscopy studies on linear polyamines, Biochem. Soc. Trans. 35 (2007) 374–380.
[22] S.M. Fiuza, A.M. Amado, H.F. dos Santos, M.P.M. Marques, L.A.E. Batista de Carvalho, Conformational and vibrational study of cis-diamminedichloropalladium(II), Phys. Chem. Chem. Phys. 12 (2010) 14309–14321.
[23] T.M. Silva, S. Oredsson, L. Persson, P. Woster, M.P.M. Marques, Novel Pt(II) and Pd(II) complexes with polyamine analogues: synthesis and vibrational analysis, J. Inorg. Biochem. 108 (2012) 1–7.
[24] A.L.M. Batista de Carvalho, S.M. Fiuza, J. Tomkinson, L.A.E. Batista de Carvalho, M.P. Marques, Pt(II) complexes with linear diamines — part I: vibrational study of Pt-diaminopropane, Spectroscopy 27 (2012), 206297 (206211 pages).
[25] S. Padrão, S.M. Fiuza, A.M. Amado, A.M. Amorim da Costa, L.A.E. Batista de Carvalho, Validation of the mPW1PW quantum chemical calculations for the vibrational study of organic molecules — re-assignment of the isopropylamine vibrational spectra, J. Phys. Org. Chem. 24 (2012) 110–121.

[26] A.M. Amado, S.M. Fiuza, L.A.E. Batista de Carvalho, P.J.A. Ribeiro-Claro, On the effects of changing Gaussian program version and SCRF defining parameters: isopropylamine as a case study, Bull. Chem. Soc. Jpn. 85 (2012) 962–975.
[27] M.P.M. Marques, R. Valero, S.F. Parker, J. Tomkinson, L.A.E. Batista de Carvalho, Polymorphism in cisplatin anticancer drug, J. Phys. Chem. B 117 (2013) 6421–6429.
[28] A.M. Amado, S.M. Fiuza, L.A.E. Batista de Carvalho, P.J.A. Ribeiro-Claro, On the relevance of considering the intermolecular interactions on the prediction of the vibrational spectra of isopropylamine, J. Chem. (2013), 682514.
[29] S.M. Fiuza, A.M. Amado, S.F. Parker, M.P.M. Marques, L.A.E. Batista de Carvalho, Conformational insights and vibrational study of a promising anticancer agent: the role of the ligand in Pd(II)-amine complexes, New J. Chem. 39 (2015) 6274–6283.
[30] M.P.M. Marques, D. Gianolio, G. Cibin, J. Tomkinson, S.F. Parker, R. Valero, R.P. Lopes, L.A.E. Batista de Carvalho, A molecular view of cisplatin's mode of action: interplay with DNA bases and acquired resistance, Phys. Chem. Chem. Phys. 17 (2015) 5155–5171.
[31] T.M. Silva, S. Andersson, S.K. Sukumaran, M.P. Marques, L. Persson, S. Oredsson, Norspermidine and novel Pd(II) and Pt(II) polynuclear complexes of norspermidine as potential antineoplastic agents against breast cancer, PLoS One 8 (2013), e55651.
[32] M.J. Frisch, G.W. Trucks, H.B. Schlegel, G.E. Scuseria, M.A. Robb, J.R. Cheeseman, G. Scalmani, V. Barone, B. Mennucci, G.A. Petersson, H. Nakatsuji, M. Caricato, X. Li, H.P. Hratchian, A.F. Izmaylov, J. Bloino, G. Zheng, J.L. Sonnenberg, M. Hada, M. Ehara, K. Toyota, R. Fukuda, J. Hasegawa, M. Ishida, T. Nakajima, Y. Honda, O. Kitao, H. Nakai, T. Vreven, J.A. Montgomery Jr., J.E. Peralta, F. Ogliaro, M. Bearpark, J.J. Heyd, E. Brothers, K.N. Kudin, V.N. Staroverov, R. Kobayashi, J. Normand, K. Raghavachari, A. Rendell, J.C. Burant, S.S. Iyengar, J. Tomasi, M. Cossi, N. Rega, J.M. Millam, M. Klene, J.E. Knox, J.B. Cross, V. Bakken, C. Adamo, J. Jaramillo, R. Gomperts, R.E. Stratmann, O. Yazyev, A.J. Austin, R. Cammi, C. Pomelli, J.W. Ochterski, R.L. Martin, K. Morokuma, V.G. Zakrzewski, G.A. Voth, P. Salvador, J.J. Dannenberg, S. Dapprich, A.D. Daniels, O. Farkas, J.B. Foresman, J.V. Ortiz, J. Cioslowski, D.J. Fox, Gaussian 09, Revision A.02, Gaussian, Inc., Wallingford CT, 2009.
[33] S.M. Fiuza, T.M. Silva, M.P.M. Marques, L.A.E.B. de Carvalho, A.M. Amado, On the correction of calculated vibrational frequencies for the effects of the counterions α,ω-diamine dihydrochlorides, J. Mol. Model. C7 - 266 (21) (2015) 1–13.
[34] J. Richardi, H. Krienke, P.H. Fries, Dielectric constants of liquid formamide, N-methylformamide and dimethylformamide via molecular Ornstein-Zernike theory, Chem. Phys. Lett. 273 (1997) 115–121.
[35] A.E. Reed, F. Weinhold, Natural localized molecular-orbitals, J. Chem. Phys. 83 (1985) 1736–1740.
[36] A.E. Reed, R.B. Weinstock, F. Weinhold, Natural-population analysis, J. Chem. Phys. 83 (1985) 735–746.
[37] A.E. Reed, L.A. Curtiss, F. Weinhold, Intermolecular interactions from a natural bond orbital, donor–acceptor viewpoint, Chem. Rev. 88 (1988) 899–926.
[38] L.A.E. Batista de Carvalho, A.M.A. da Costa, M.L. Duarte, J.J.C. Teixeira-Dias, Conformational studies of n-propylamine by combined ab initio MO calculations and Raman spectroscopy, Spectrochim. Acta A44 (1988) 723–732.
[39] L.A.E. Batista de Carvalho, L.E. Lourenço, M.P.M. Marques, Conformational study of 1,2-diaminoethane by combined ab initio MO calculations and Raman spectroscopy, J. Mol. Struct. 482&483 (1999) 639–646.
[40] L.A.E. Batista de Carvalho, J.J.C. Teixeira-Dias, Raman spectra, conformational stability and normal coordinate analysis of ethylmethylamine, J. Raman Spectrosc. 26 (1995) 653–661.
[41] L.A.E. Batista de Carvalho, J.J.C. Teixeira-Dias, R. Fausto, A molecular mechanics force field for conformational analysis of aliphatic acyclic amines, Struct. Chem. 1 (1990) 533–542.
[42] L.A.E. Batista de Carvalho, J.J.C. Teixeira-Dias, Conformational analysis of dimethylethylamine: an ab initio MO study and comparison with ethylamine and ethylmethylamine, J. Mol. Struct. (THEOCHEM) 282 (1993) 211–221.
[43] P.L. Huyskens, Factors governing influence of a 1st hydrogen-bond on formation of a 2nd one by same molecule or ion, J. Am. Chem. Soc. 99 (1977) 2578–2582.
[44] I.A.W. Filot, A.R.A. Palmans, P.A.J. Hilbers, R.A. van Santen, E.A. Pidko, T.F.A. de Greef, Understanding cooperativity in hydrogen-bond-induced supramolecular polymerization: a density functional theory study, J. Phys. Chem. B 114 (2010) 13667–13674.
[45] E.M. Cabaleiro-Lago, M.A. Ríos, Ab initio study of interactions in methylamine clusters. The significance of cooperative effects, J. Chem. Phys. 112 (2000) 2155–2163.
[46] E.M. Cabaleiro-Lago, M.A. Ríos, An ab initio study of the interaction in dimethylamine dimer and trimer, J. Chem. Phys. 113 (2000) 9523–9531.
[47] M.M. Nolasco, A.M. Amado, P.J.A. Ribeiro-Claro, Effect of hydrogen bonding in the vibrational spectra of *trans*-cinnamic acid, J. Raman Spectrosc. 40 (2009) 394–400.
[48] G.A. Giffin, S. Boesch, D.N. Bopege, D.R. Powell, R.A. Wheeler, R. Frech, Vibrational spectroscopy of secondary amine salts: 1. Assignment of NH_2^+ stretching frequencies in crystalline phases, J. Phys. Chem. B 113 (2009) 15914–15920.
[49] R. Dennington, T. Keith, J. Millam, GaussView, Version 5, Gaussian, Inc., Shawnee Mission KS, 2009.
[50] L.J. Bellamy, The Infrared Spectra of Complex Molecules, third ed. Chapman and Hall Ltd., London, 1975.
[51] L. Choongkeun, P. Sun-Kyung, M. Kyung-Chul, K. Yunsoo, L. Nam-Soo, Vibrational analysis and intermolecular hydrogen bonding of azodicarbonamide in the pentamer cluster, Bull. Kor. Chem. Soc. 29 (2008) 1951–1959.
[52] J.P. Merrick, D. Moran, L. Radom, An evaluation of harmonic vibrational frequency scale factors, J. Phys. Chem. A 111 (2007) 11683–11700.
[53] N.B. Coulthup, L.H. Daly, S.E. Wiberley, Introduction to Infrared and Raman Spectroscopy, third ed. Academic Press, INC, San Diego, 1990.
[54] B. Stuart, Biological Applications of Infrared Spectroscopy, third ed. John Wiley & Sons, Ltd, West Sussex, 1997.
[55] H. Günzler, H.-U. Gremlich, IR Spectroscopy — an Introduction, first ed. Weinheim, Wiley-VCH Verlag GmbH, 2002.
[56] L.A.E. Batista de Carvalho, A.M.A. Da Costa, J.J.C. Teixeira-Dias, E.F.G. Barbosa, I.M.S. Lampreia, Temperature-dependent intensities of Raman bands of di-n-butylamine, J. Raman Spectrosc. 18 (1987) 115–118.